DESY 03-015

February 2003

Dijet angular distributions in photoproduction of charm at HERA

ZEUS Collaboration

arXiv:hep-ex/0302025 v2 10 Jul 2003

Abstract

Dijet angular distributions of photoproduction events in which a $D^{*\pm}$ meson is produced in association with one of two energetic jets have been measured with the ZEUS detector at HERA, using an integrated luminosity of 120 pb^{-1}. Differential cross sections as a function of the angle between the charm-jet and the proton-beam direction in the dijet rest frame have been measured for samples enriched in direct or resolved photon events. The results are compared with predictions from leading-order parton-shower Monte Carlo models and with next-to-leading-order QCD calculations. The angular distributions show clear evidence for the existence of charm originating from the photon.

The ZEUS Collaboration

S. Chekanov, M. Derrick, D. Krakauer, J.H. Loizides[1], S. Magill, B. Musgrave, J. Repond, R. Yoshida
Argonne National Laboratory, Argonne, Illinois 60439-4815 [n]

M.C.K. Mattingly
Andrews University, Berrien Springs, Michigan 49104-0380

P. Antonioli, G. Bari, M. Basile, L. Bellagamba, D. Boscherini, A. Bruni, G. Bruni, G. Cara Romeo, L. Cifarelli, F. Cindolo, A. Contin, M. Corradi, S. De Pasquale, P. Giusti, G. Iacobucci, A. Margotti, R. Nania, F. Palmonari, A. Pesci, G. Sartorelli, A. Zichichi
University and INFN Bologna, Bologna, Italy [e]

G. Aghuzumtsyan, D. Bartsch, I. Brock, S. Goers, H. Hartmann, E. Hilger, P. Irrgang, H.-P. Jakob, A. Kappes[2], U.F. Katz[2], O. Kind, U. Meyer, E. Paul[3], J. Rautenberg, R. Renner, A. Stifutkin, J. Tandler, K.C. Voss, M. Wang, A. Weber[4]
Physikalisches Institut der Universität Bonn, Bonn, Germany [b]

D.S. Bailey[5], N.H. Brook[5], J.E. Cole, B. Foster, G.P. Heath, H.F. Heath, S. Robins, E. Rodrigues[6], J. Scott, R.J. Tapper, M. Wing
H.H. Wills Physics Laboratory, University of Bristol, Bristol, United Kingdom [m]

M. Capua, A. Mastroberardino, M. Schioppa, G. Susinno
Calabria University, Physics Department and INFN, Cosenza, Italy [e]

J.Y. Kim, Y.K. Kim, J.H. Lee, I.T. Lim, M.Y. Pac[7]
Chonnam National University, Kwangju, Korea [g]

A. Caldwell[8], M. Helbich, X. Liu, B. Mellado, Y. Ning, S. Paganis, Z. Ren, W.B. Schmidke, F. Sciulli
Nevis Laboratories, Columbia University, Irvington on Hudson, New York 10027 [o]

J. Chwastowski, A. Eskreys, J. Figiel, K. Olkiewicz, P. Stopa, L. Zawiejski
Institute of Nuclear Physics, Cracow, Poland [i]

L. Adamczyk, T. Bołd, I. Grabowska-Bołd, D. Kisielewska, A.M. Kowal, M. Kowal, T. Kowalski, M. Przybycień, L. Suszycki, D. Szuba, J. Szuba[9]
Faculty of Physics and Nuclear Techniques, University of Mining and Metallurgy, Cracow, Poland [p]

A. Kotański[10], W. Słomiński[11]
Department of Physics, Jagellonian University, Cracow, Poland

L.A.T. Bauerdick[12], U. Behrens, I. Bloch, K. Borras, V. Chiochia, D. Dannheim, G. Drews, J. Fourletova, U. Fricke, A. Geiser, F. Goebel[8], P. Göttlicher[13], O. Gutsche, T. Haas, W. Hain, G.F. Hartner, S. Hillert, B. Kahle, U. Kötz, H. Kowalski[14], G. Kramberger, H. Labes, D. Lelas, B. Löhr, R. Mankel, I.-A. Melzer-Pellmann, M. Moritz[15], C.N. Nguyen, D. Notz, M.C. Petrucci[16], A. Polini, A. Raval, U. Schneekloth, F. Selonke[3], H. Wessoleck, G. Wolf, C. Youngman, W. Zeuner
Deutsches Elektronen-Synchrotron DESY, Hamburg, Germany

S. Schlenstedt
DESY Zeuthen, Zeuthen, Germany

G. Barbagli, E. Gallo, C. Genta, P. G. Pelfer
University and INFN, Florence, Italy [e]

A. Bamberger, A. Benen, N. Coppola
Fakultät für Physik der Universität Freiburg i.Br., Freiburg i.Br., Germany [b]

M. Bell, P.J. Bussey, A.T. Doyle, C. Glasman, J. Hamilton, S. Hanlon, S.W. Lee, A. Lupi, D.H. Saxon, I.O. Skillicorn
Department of Physics and Astronomy, University of Glasgow, Glasgow, United Kingdom [m]

I. Gialas
Department of Engineering in Management and Finance, Univ. of Aegean, Greece

B. Bodmann, T. Carli, U. Holm, K. Klimek, N. Krumnack, E. Lohrmann, M. Milite, H. Salehi, S. Stonjek[17], K. Wick, A. Ziegler, Ar. Ziegler
Hamburg University, Institute of Exp. Physics, Hamburg, Germany [b]

C. Collins-Tooth, C. Foudas, R. Gonçalo[6], K.R. Long, A.D. Tapper
Imperial College London, High Energy Nuclear Physics Group, London, United Kingdom [m]

P. Cloth, D. Filges
Forschungszentrum Jülich, Institut für Kernphysik, Jülich, Germany

M. Kuze, K. Nagano, K. Tokushuku[18], S. Yamada, Y. Yamazaki
Institute of Particle and Nuclear Studies, KEK, Tsukuba, Japan [f]

A.N. Barakbaev, E.G. Boos, N.S. Pokrovskiy, B.O. Zhautykov
Institute of Physics and Technology of Ministry of Education and Science of Kazakhstan, Almaty, Kazakhstan

H. Lim, D. Son
Kyungpook National University, Taegu, Korea [g]

K. Piotrzkowski
Institut de Physique Nucléaire, Université Catholique de Louvain, Louvain-la-Neuve, Belgium

F. Barreiro, O. González, L. Labarga, J. del Peso, E. Tassi, J. Terrón, M. Vázquez
Departamento de Física Teórica, Universidad Autónoma de Madrid, Madrid, Spain [l]

M. Barbi, F. Corriveau, S. Gliga, J. Lainesse, S. Padhi, D.G. Stairs
Department of Physics, McGill University, Montréal, Québec, Canada H3A 2T8 [a]

T. Tsurugai
Meiji Gakuin University, Faculty of General Education, Yokohama, Japan

A. Antonov, P. Danilov, B.A. Dolgoshein, D. Gladkov, V. Sosnovtsev, S. Suchkov
Moscow Engineering Physics Institute, Moscow, Russia [j]

R.K. Dementiev, P.F. Ermolov, Yu.A. Golubkov, I.I. Katkov, L.A. Khein, I.A. Korzhavina, V.A. Kuzmin, B.B. Levchenko[19], O.Yu. Lukina, A.S. Proskuryakov, L.M. Shcheglova, N.N. Vlasov, S.A. Zotkin
Moscow State University, Institute of Nuclear Physics, Moscow, Russia [k]

N. Coppola, S. Grijpink, E. Koffeman, P. Kooijman, E. Maddox, A. Pellegrino, S. Schagen, H. Tiecke, N. Tuning, J.J. Velthuis, L. Wiggers, E. de Wolf
NIKHEF and University of Amsterdam, Amsterdam, Netherlands [h]

N. Brümmer, B. Bylsma, L.S. Durkin, T.Y. Ling
Physics Department, Ohio State University, Columbus, Ohio 43210 [n]

S. Boogert, A.M. Cooper-Sarkar, R.C.E. Devenish, J. Ferrando, G. Grzelak, S. Patel, M. Rigby, M.R. Sutton, R. Walczak
Department of Physics, University of Oxford, Oxford United Kingdom [m]

A. Bertolin, R. Brugnera, R. Carlin, F. Dal Corso, S. Dusini, A. Garfagnini, S. Limentani, A. Longhin, A. Parenti, M. Posocco, L. Stanco, M. Turcato
Dipartimento di Fisica dell' Università and INFN, Padova, Italy [e]

E.A. Heaphy, F. Metlica, B.Y. Oh, P.R.B. Saull[20], J.J. Whitmore[21]
Department of Physics, Pennsylvania State University, University Park, Pennsylvania 16802 [o]

Y. Iga
Polytechnic University, Sagamihara, Japan [f]

G. D'Agostini, G. Marini, A. Nigro
Dipartimento di Fisica, Università 'La Sapienza' and INFN, Rome, Italy [e]

C. Cormack[22], J.C. Hart, N.A. McCubbin
Rutherford Appleton Laboratory, Chilton, Didcot, Oxon, United Kingdom [m]

C. Heusch
University of California, Santa Cruz, California 95064 [n]

I.H. Park
Department of Physics, Ewha Womans University, Seoul, Korea

N. Pavel
Fachbereich Physik der Universität-Gesamthochschule Siegen, Germany

H. Abramowicz, A. Gabareen, S. Kananov, A. Kreisel, A. Levy
Raymond and Beverly Sackler Faculty of Exact Sciences, School of Physics, Tel-Aviv University, Tel-Aviv, Israel [d]

T. Abe, T. Fusayasu, S. Kagawa, T. Kohno, T. Tawara, T. Yamashita
Department of Physics, University of Tokyo, Tokyo, Japan [f]

R. Hamatsu, T. Hirose[3], M. Inuzuka, S. Kitamura[23], K. Matsuzawa, T. Nishimura
Tokyo Metropolitan University, Department of Physics, Tokyo, Japan [f]

M. Arneodo[24], M.I. Ferrero, V. Monaco, M. Ruspa, R. Sacchi, A. Solano
Università di Torino, Dipartimento di Fisica Sperimentale and INFN, Torino, Italy [e]

T. Koop, G.M. Levman, J.F. Martin, A. Mirea
Department of Physics, University of Toronto, Toronto, Ontario, Canada M5S 1A7 [a]

J.M. Butterworth, C. Gwenlan, R. Hall-Wilton, T.W. Jones, M.S. Lightwood, B.J. West
Physics and Astronomy Department, University College London, London, United Kingdom [m]

J. Ciborowski[25], R. Ciesielski[26], R.J. Nowak, J.M. Pawlak, J. Sztuk[27], T. Tymieniecka[28], A. Ukleja[28], J. Ukleja, A.F. Żarnecki
Warsaw University, Institute of Experimental Physics, Warsaw, Poland [q]

M. Adamus, P. Plucinski
Institute for Nuclear Studies, Warsaw, Poland [q]

Y. Eisenberg, L.K. Gladilin[29], D. Hochman, U. Karshon
Department of Particle Physics, Weizmann Institute, Rehovot, Israel [c]

D. Kçira, S. Lammers, L. Li, D.D. Reeder, A.A. Savin, W.H. Smith
Department of Physics, University of Wisconsin, Madison, Wisconsin 53706 [n]

A. Deshpande, S. Dhawan, V.W. Hughes, P.B. Straub
Department of Physics, Yale University, New Haven, Connecticut 06520-8121 [n]

S. Bhadra, C.D. Catterall, S. Fourletov, S. Menary, M. Soares, J. Standage
Department of Physics, York University, Ontario, Canada M3J 1P3 [a]

[1] also affiliated with University College London
[2] on leave of absence at University of Erlangen-Nürnberg, Germany
[3] retired
[4] self-employed
[5] PPARC Advanced fellow
[6] supported by the Portuguese Foundation for Science and Technology (FCT)
[7] now at Dongshin University, Naju, Korea
[8] now at Max-Planck-Institut für Physik, München/Germany
[9] partly supported by the Israel Science Foundation and the Israel Ministry of Science
[10] supported by the Polish State Committee for Scientific Research, grant no. 2 P03B 09322
[11] member of Dept. of Computer Science
[12] now at Fermilab, Batavia/IL, USA
[13] now at DESY group FEB
[14] on leave of absence at Columbia Univ., Nevis Labs., N.Y./USA
[15] now at CERN
[16] now at INFN Perugia, Perugia, Italy
[17] now at Univ. of Oxford, Oxford/UK
[18] also at University of Tokyo
[19] partly supported by the Russian Foundation for Basic Research, grant 02-02-81023
[20] now at National Research Council, Ottawa/Canada
[21] on leave of absence at The National Science Foundation, Arlington, VA/USA
[22] now at Univ. of London, Queen Mary College, London, UK
[23] present address: Tokyo Metropolitan University of Health Sciences, Tokyo 116-8551, Japan
[24] also at Università del Piemonte Orientale, Novara, Italy
[25] also at Lódź University, Poland
[26] supported by the Polish State Committee for Scientific Research, grant no. 2 P03B 07222
[27] Łódź University, Poland
[28] supported by German Federal Ministry for Education and Research (BMBF), POL 01/043
[29] on leave from MSU, partly supported by University of Wisconsin via the U.S.-Israel BSF

[a] supported by the Natural Sciences and Engineering Research Council of Canada (NSERC)

[b] supported by the German Federal Ministry for Education and Research (BMBF), under contract numbers HZ1GUA 2, HZ1GUB 0, HZ1PDA 5, HZ1VFA 5

[c] supported by the MINERVA Gesellschaft für Forschung GmbH, the Israel Science Foundation, the U.S.-Israel Binational Science Foundation and the Benozyio Center for High Energy Physics

[d] supported by the German-Israeli Foundation and the Israel Science Foundation

[e] supported by the Italian National Institute for Nuclear Physics (INFN)

[f] supported by the Japanese Ministry of Education, Science and Culture (the Monbusho) and its grants for Scientific Research

[g] supported by the Korean Ministry of Education and Korea Science and Engineering Foundation

[h] supported by the Netherlands Foundation for Research on Matter (FOM)

[i] supported by the Polish State Committee for Scientific Research, grant no. 620/E-77/SPUB-M/DESY/P-03/DZ 247/2000-2002

[j] partially supported by the German Federal Ministry for Education and Research (BMBF)

[k] supported by the Fund for Fundamental Research of Russian Ministry for Science and Education and by the German Federal Ministry for Education and Research (BMBF)

[l] supported by the Spanish Ministry of Education and Science through funds provided by CICYT

[m] supported by the Particle Physics and Astronomy Research Council, UK

[n] supported by the US Department of Energy

[o] supported by the US National Science Foundation

[p] supported by the Polish State Committee for Scientific Research, grant no. 112/E-356/SPUB-M/DESY/P-03/DZ 301/2000-2002, 2 P03B 13922

[q] supported by the Polish State Committee for Scientific Research, grant no. 115/E-343/SPUB-M/DESY/P-03/DZ 121/2001-2002, 2 P03B 07022

1 Introduction

High-energy collisions at the HERA ep collider between a quasi-real photon and a proton provide an effective source of photoproduction processes. Jets with high transverse energy and/or charm (c) quarks produced in such processes can be described within quantum chromodynamics (QCD) in two sub-classes: direct processes are those in which the photon couples as a point-like object in the hard scattering; resolved processes are those in which the photon acts as a source of incoming partons, one of which participates in the hard interaction. Both processes can lead to two jets in the final state. Samples enriched in direct and resolved photon events can be identified using the variable $x_\gamma^{\rm obs}$ [1], which is the fraction of the photon's momentum contributing to the production of the two jets.

Inclusive cross sections for photoproduction of $D^{*\pm}(2010)$ mesons as well as cross sections for "charm dijet" events, in which the D^* is observed in events with two energetic jets, have been previously reported [2]. Differential cross sections of the D^* and associated dijet system are larger than next-to-leading-order (NLO) QCD predictions [3] at low $x_\gamma^{\rm obs}$, but are in agreement at high $x_\gamma^{\rm obs}$. The data were also compared to predictions of leading-logarithmic parton-shower Monte Carlo (MC) models. According to these comparisons, about 60% of the events can be attributed to the direct photon-gluon-fusion (PGF) process $\gamma g \to c\bar{c}$, illustrated in Fig. 1a). The MC models predict that most of the resolved photon events come from charm excitation of the photon (Figs. 1c) and 1d)) rather than from the $gg \to c\bar{c}$ process (Fig. 1b)). The aim of this analysis is to determine the dominant mechanisms for charm dijet photoproduction in both direct and resolved photon processes.

Measuring the angular distribution of the outgoing jets allows the dominant subprocesses to be determined and the MC predictions to be tested, as was done previously [4] for inclusive dijet events. This study showed that the differential cross-section $d\sigma/d|\cos\theta^*|$, where θ^* is the angle between the jet-jet axis and the proton beam direction in the dijet rest frame, is sensitive to the spin of the propagator in the hard subprocess. In direct photon processes, in which the propagator in the leading-order (LO) QCD diagrams is a quark, the differential cross section rises slowly towards high $|\cos\theta^*|$ values ($d\sigma/d|\cos\theta^*| \approx (1-|\cos\theta^*|)^{-1}$). In resolved photon processes, the gluon propagator is allowed at LO and dominates over the quark propagator due to the stronger gluon-gluon coupling compared to the quark-gluon coupling. In this case the cross section rises steeply when $|\cos\theta^*|$ increases ($d\sigma/d|\cos\theta^*| \approx (1-|\cos\theta^*|)^{-2}$). Similar results have been reported in photon-photon collisions [5].

If most of the resolved-photon charm dijet events are produced as a result of charm from the photon, a gluon-exchange contribution, as seen in Fig. 1d), should dominate. This results in a steep rise of the cross section towards high $|\cos\theta^*|$ values. The other diagrams of Fig. 1 involve quark exchange and thus should not show such a sharp rise. If one of

the jets is explicitly tagged as a charm jet, the sign of $\cos\theta^*$ can be defined. If the charm originates from the photon, the charm jet generally lies in the photon hemisphere.

2 Experimental conditions

The analysis was performed using data collected with the ZEUS detector at HERA during 1996 – 2000. In this period, HERA collided electrons or positrons with energy $E_e = 27.5\,\text{GeV}$ and protons with energy $E_p = 820\,\text{GeV}$ (1996 – 1997) or $E_p = 920\,\text{GeV}$ (1998 – 2000), corresponding to integrated luminosities of 38.6 ± 0.6 and 81.9 ± 1.8 pb^{-1} and to centre-of-mass energies $\sqrt{s} = 300\,\text{GeV}$ and $\sqrt{s} = 318\,\text{GeV}$, respectively. This data sample is about a factor of three larger than that used for the previous charm dijet analysis [2].

A detailed description of the ZEUS detector can be found elsewhere [6]. A brief outline of the components that are most relevant for this analysis is given below.

Charged particles are tracked in the central tracking detector (CTD) [7], which operates in a magnetic field of 1.43 T provided by a thin superconducting coil. The CTD consists of 72 cylindrical drift chamber layers, organized in 9 superlayers covering the polar-angle[1] region $15° < \theta < 164°$. The transverse-momentum resolution for full-length tracks is $\sigma(p_T)/p_T = 0.0058p_T \oplus 0.0065 \oplus 0.0014/p_T$ (p_T in GeV).

The high-resolution uranium–scintillator calorimeter (CAL) [8] consists of three parts: the forward (FCAL), the barrel (BCAL) and the rear (RCAL) calorimeters. Each part is subdivided transversely into towers and longitudinally into one electromagnetic section (EMC) and either one (in RCAL) or two (in BCAL and FCAL) hadronic sections (HAC). The smallest subdivision of the calorimeter is called a cell. The CAL energy resolutions, as measured under test-beam conditions, are $\sigma(E)/E = 0.18/\sqrt{E}$ for electrons and $\sigma(E)/E = 0.35/\sqrt{E}$ for hadrons (E in GeV).

The luminosity was measured from the rate of the bremsstrahlung process $e^+p \rightarrow e^+\gamma p$, where the photon was measured in a lead-scintillator calorimeter [9] placed in the HERA tunnel at $Z = -107$ m.

[1] The ZEUS coordinate system is a right-handed Cartesian system, with the Z axis pointing in the proton beam direction, referred to as the "forward direction", and the X axis pointing left towards the centre of HERA. The coordinate origin is at the nominal interaction point. The pseudorapidity is defined as $\eta = -\ln\left(\tan\frac{\theta}{2}\right)$, where the polar angle, θ, is measured with respect to the proton beam direction.

3 Event selection

Photoproduction events were selected with a three-level trigger [6, 10]. The inclusive photoproduction sample was defined by requiring a reconstructed vertex and no scattered electron or positron found in the CAL, thus restricting the photon virtuality, Q^2, to be below 1 GeV^2, with median $Q^2 \approx 3 \cdot 10^{-4}$ GeV^2. The photon-proton centre-of-mass energy, W, was restricted to the range $130 < W < 280$ GeV. The latter was measured using the Jacquet-Blondel [11] estimator $W_{\rm JB} = \sqrt{4 y_{\rm JB} E_e E_p}$, where $y_{\rm JB} = \Sigma_i (E_i - p_{Z,i})/2E_e$, the sum runs over all CAL cells and $p_{Z,i}$ is the Z component of the momentum vector assigned to each cell of energy E_i. Jets were reconstructed with the k_T cluster algorithm [12] in its longitudinally invariant inclusive mode [13]. The events were required to have at least two jets[2] with pseudorapidity $|\eta^{\rm jet}| < 2.4$ and transverse energy $E_T^{\rm jet} > 5$ GeV. The measured jet energies as well as $W_{\rm JB}$ were corrected for energy losses in inactive material in front of the CAL, using the MC simulation.

The D^* mesons were reconstructed using the mass-difference technique applied to the decay chain[3] $D^{*\pm} \to D^0 \pi_S^\pm \to K^\mp \pi^\pm \pi_S^\pm$. Tracks in the CTD with opposite charges and transverse momenta $p_T > 0.5$ GeV were combined in pairs to form D^0 candidates. Kaon and pion masses were assumed in turn for each track to calculate the pair invariant mass, $M(K\pi)$. A third track, π_S, assumed to be the "soft pion" from the D^* decay, with $p_T > 0.15$ GeV and a charge opposite to the kaon, was added to form a D^* candidate. Events with a mass difference $\Delta M = M(K\pi\pi_s) - M(K\pi)$ in the range $0.1435 < \Delta M < 0.1475$ GeV around the nominal value [14] and the range $1.81 < M(K\pi) < 1.92$ GeV around the D^0 mass were called D^* candidates. To suppress combinatorial background, a cut $p_T^{D^*}/E_T^{\theta>10^\circ} > 0.15$ was applied [2], where $E_T^{\theta>10^\circ}$ is the transverse energy measured in the CAL outside a cone of $\theta = 10^\circ$ in the forward direction. The reconstructed D^* mesons were required to have $p_T^{D^*} > 3$ GeV and pseudorapidity in the range $|\eta^{D^*}| < 1.5$.

These cuts ensure that the events lie in a well understood acceptance region of the detector.

4 Jet kinematic variables

Samples enriched in direct and resolved photon events were separated by a selection on the variable

$$x_\gamma^{\rm obs} = \frac{\Sigma_{\rm jets}\left(E_T^{\rm jet}\ e^{-\eta^{\rm jet}}\right)}{2yE_e},$$

[2] The fraction of events with more than two jets is 11%.

[3] Throughout this article, D^0 refers to both D^0 and $\bar{D}^0$.

where yE_e is the initial photon energy and the sum is over the two jets with the highest $E_T^{\rm jet}$. The selection of $x_\gamma^{\rm obs} > 0.75$ and $x_\gamma^{\rm obs} < 0.75$ yields samples enriched in direct and resolved photon processes, respectively.

A complementary variable is

$$x_p^{\rm obs} = \frac{\Sigma_{\rm jets}\left(E_T^{\rm jet}\ e^{\eta^{\rm jet}}\right)}{2E_p},$$

which is the fraction of the proton's momentum contributing to the production of the two jets.

The dijet scattering angle, θ^*, is reconstructed using

$$\cos\theta^* = \tanh\left(\frac{\eta^{\rm jet1} - \eta^{\rm jet2}}{2}\right). \tag{1}$$

In the simple case in which two jets are back-to-back in the transverse plane and have equal transverse energies, the dijet invariant mass is given by $M_{\rm jj} = 2E_T^{\rm jet}/\sqrt{1-|\cos\theta^*|^2}$. Therefore, for a given $M_{\rm jj}$, events with high values of $|\cos\theta^*|$ have lower $E_T^{\rm jet}$. In order to study the $|\cos\theta^*|$ distribution up to $|\cos\theta^*| = 0.83$ without bias from the $E_T^{\rm jet}$ cut, $M_{\rm jj}$ was required to be above 18 GeV.

A cut on the average longitudinal boost, $\bar{\eta} = (\eta^{\rm jet1} + \eta^{\rm jet2})/2$, of $|\bar{\eta}| < 0.7$ was applied. This selection limits $\eta^{\rm jet}$ to $|\eta^{\rm jet}| < 1.9$ and removes the bias caused by the explicit cuts on $\eta^{\rm jet}$ [4]. It also reduces the bias caused by the cut on $|\eta^{D^*}| < 1.5$ while retaining a sufficiently large number of events. Monte Carlo studies show that the residual distortion due to the $|\eta^{D^*}|$ cut is small and confined to the extreme bins of the $\cos\theta^*$ distribution.

These cuts ensure that any features seen in the measured distributions can be attributed to the dynamics of the hard scattering processes.

5 Models and QCD calculations

The MC simulation programs PYTHIA 6.156 [15] and HERWIG 6.301 [16] were used to model the final states. The PYTHIA and HERWIG simulations use on-shell LO matrix elements for charm photoproduction processes. Higher-order QCD effects are simulated in the leading-logarithmic approximation with initial- and final-state radiation obeying DGLAP evolution [17]. Coherence effects from soft-gluon interference are included. The parton density functions (PDF) CTEQ5L [18] for the proton and GRV-G LO [19] for the

photon were used. The LO direct and resolved photon processes were generated proportionally to their predicted MC cross sections, using charm- and beauty-quark masses of $m_c = 1.5\,\text{GeV}$ and $m_b = 4.75\,\text{GeV}$, respectively. Fragmentation into hadrons is simulated in HERWIG with a cluster algorithm [20] and in PYTHIA with the Lund string model [21].

Samples of MC events larger than the dataset were produced. To calculate the acceptances and to estimate hadronisation effects, the events were passed through the GEANT 3.13-based [22] simulation of the ZEUS detector and trigger. They were reconstructed and analysed by the same program chain as the data. Samples corresponding to different data taking conditions were generated in proportion to their luminosities. For PYTHIA, in addition to the D^* decay chain used for this analysis, background events that arise from other $D^{*\pm}$ decay modes or similar decay modes of other charm mesons were also simulated.

The MC event generator CASCADE 1.00/09 [23] simulates heavy-quark photoproduction in the framework of the semi-hard or k_t-factorisation approach [24]. The matrix element used in CASCADE is the off-shell LO PGF process. The CASCADE initial-state radiation is based on CCFM evolution [25], which includes in the perturbative expansion the $\ln(1/x)$ terms in addition to the $\ln Q^2$ terms used in DGLAP evolution. To simulate final-state radiation, CASCADE uses PYTHIA 6.1 and the fragmentation into hadrons is simulated with the Lund string model. The cross section is calculated by convoluting the off-shell PGF matrix element with the unintegrated gluon density of the proton obtained from the CCFM fit to the HERA F_2 data, by fixing most of the free parameters [23]. Although the CASCADE matrix element corresponds to the off-shell PGF direct photon process only (Fig. 1a)), resolved photon processes are reproduced by the CCFM initial-state radiation [26].

The NLO QCD calculations of differential cross sections for photoproduction of charm dijet events in the HERA kinematic region are available [3] in the fixed-order (FO) scheme. The PDF parameterisations used were CTEQ5M1 [18] for the proton and AFGHO [27] for the photon. The factorisation scales of the photon and proton PDFs, μ_F, and the renormalisation scale, μ_R, used for the calculation were set to $\mu_F = \mu_R = m_T \equiv \sqrt{m_c^2 + \langle p_T^2 \rangle}$, where $\langle p_T^2 \rangle$ was set to the average p_T^2 of the charm quark and antiquark. The charm fragmentation into D^* was performed using the Peterson fragmentation function [28] with an ϵ parameter of 0.035 [29].

In all cases, the fraction of c quarks fragmenting into a D^* was assumed to be 0.235 [30] and a charm quark mass of $m_c = 1.5\,\text{GeV}$ was used.

6 Results

The ΔM distribution for dijet events in the D^0 signal region shows a clear D^* signal. The analysis is based on 1092 ± 43 $D^{*\pm}$ mesons found in the $0.1435 < \Delta M < 0.1475\,\text{GeV}$ region over a background of 328 events. The signal has similar characteristics as that in the previous ZEUS publication [2] except that the signal to background ratio has improved by a factor of three due to the tighter cuts (see Sections 3 and 4) used here. The background was determined from the ΔM distribution for wrong-charge combinations, where the tracks forming D^0 candidates had the same charge and the π_S had the opposite charge.

The number of events in each bin of the measured variables was extracted by performing a bin-by-bin wrong-charge background subtraction. To obtain differential cross sections, each value was then multiplied by a correction factor proportional to the ratio of generated to reconstructed events from the PYTHIA MC simulation. The measured cross sections are the luminosity-weighted average of the cross sections at the centre-of-mass energies $\sqrt{s} = 300$ GeV and $\sqrt{s} = 318$ GeV.

The systematic uncertainties were determined by adding the contributions from several sources in quadrature. The largest contributions were associated with the cuts on W and with the difference between the correction factors evaluated using HERWIG rather than PYTHIA. The uncertainties due to the knowledge of the CAL energy scale ($\pm 3\%$) are highly correlated between bins and are therefore shown separately. Statistical uncertainties dominate over systematic ones in most bins. The measured cross sections and their uncertainties are given in Tables 1-4.

The differential cross section as a function of x_γ^{obs} is shown in Fig. 2. The peak at high values of x_γ^{obs} indicates a large contribution from direct photon processes, but there is also a sizeable contribution from resolved photon processes at lower x_γ^{obs} values. Figure 3 shows the differential cross section as a function of x_p^{obs}. The x_p^{obs} range of the data is concentrated in the region $0.0055 < x_p^{\text{obs}} < 0.044$, where the proton PDFs are well determined.

Figure 4 shows the differential cross sections as a function of $|\cos\theta^*|$ separately for the resolved-enriched ($x_\gamma^{\text{obs}} < 0.75$) and direct-enriched ($x_\gamma^{\text{obs}} > 0.75$) samples. The cross section for the sample enriched in resolved photons exhibits a more rapid rise towards high values of $|\cos\theta^*|$ than does the cross section for the sample enriched in direct photons. Consequently, the LO subprocess $gg \to c\bar{c}$ (Fig. 1b)), with q-exchange in the t channel, cannot be the dominant resolved photon process for charm dijet events. This observation suggests a large gluon-exchange contribution originating from a charm-excitation process.

The $|\cos\theta^*|$ distributions of Fig. 4 are similar in shape to the previously reported dijet angular distributions [4], which did not require the presence of charm. In those analyses,

only the absolute value of $\cos\theta^*$ was determined. In the present study, the two jets were distinguished by associating the D^* meson to the closest jet in $\eta-\phi$ space. The associated jet is defined to be the jet with the smallest $R_i = \sqrt{(\eta^{\mathrm{jet},i} - \eta^{D^*})^2 + (\phi^{\mathrm{jet},i} - \phi^{D^*})^2}$; $(i = 1, 2)$ and with $R < 1$, where ϕ^{jet} (ϕ^{D^*}) is the azimuthal angle of the jet (D^*) in the laboratory frame. Calling this "D^* jet" jet 1 in Eq. (1), the rise of $d\sigma/d\cos\theta^*$ can be studied separately for the photon and proton directions. Figure 5 shows the differential cross sections as a function of $\cos\theta^*$ for the resolved- and direct-enriched samples. Events that did not satisfy the requirement $R < 1$ for at least one of the two jets (8.7% for $x_\gamma^{\mathrm{obs}} < 0.75$ and 1.1% for $x_\gamma^{\mathrm{obs}} > 0.75$) were not included in these $\cos\theta^*$ distributions. The PYTHIA estimation of the contribution of the direct process to the resolved-enriched sample, $x_\gamma^{\mathrm{obs}} < 0.75$, and the resolved process to the direct-enriched sample, $x_\gamma^{\mathrm{obs}} > 0.75$, are also indicated.

Direct photon events originating from the dominant q-exchange process $\gamma g \to c\bar{c}$ (Fig. 1a)) should have a distribution symmetric in $\cos\theta^*$. The angular distribution of direct-enriched events ($x_\gamma^{\mathrm{obs}} > 0.75$) exhibits a slight asymmetry, which can be explained by the feedthrough from resolved photon processes near $\cos\theta^* = -1$, as predicted by PYTHIA (Fig. 5b)).

The sample enriched in resolved photons (Fig. 5a,c)) exhibits a mild rise in the proton hemisphere towards $\cos\theta^* = 1$, consistent with expectations from quark exchange. In contrast, they have a strong rise towards $\cos\theta^* = -1$, i.e. in the photon direction, consistent with a dominant contribution from gluon exchange. For the latter case, the charm quark emerges in the photon hemisphere (Fig. 1d)). Gluon-exchange diagrams with this topology can only come, at LO, from the processes $c^\gamma g^p \to cg$ and $c^\gamma q^p \to cq$, where the superscripts refer to an origin in either the photon or proton. The partonic cross sections for these $2 \to 2$ subprocesses are highly asymmetric in $\cos\theta^*$ and show a steep rise towards the photon direction, while the subprocess $gg \to c\bar{c}$ (Fig. 1b)) is symmetric in $\cos\theta^*$. This observation suggests that the source of the LO gluon-exchange contribution as seen in Figs. 4a) and c) is charm originating from the photon. This is consistent with the MC prediction [2] that most of the resolved photon contribution to charm dijet events at HERA is due to charm originating from the photon.

7 Comparisons with theoretical predictions

7.1 Comparison with MC predictions

Figures 2–5 compare the distributions of the data with those of the MC simulations PYTHIA, HERWIG and CASCADE. For PYTHIA and HERWIG, the predictions are

normalised to the data with normalisation factors shown in brackets within the figures. For a shape comparison, the prediction for CASCADE is shown in Fig. 2 normalised to the data. Since there is a hope [31] that higher-order corrections to k_t-factorised calculations might be smaller than those to LO parton-shower calculations using DGLAP evolution, the absolute predictions from CASCADE for the differential cross sections are shown in Figs. 3 – 5.

The shapes of all data distributions are well reproduced by PYTHIA. The HERWIG predictions give an adequate description of the shapes in the data, although the rise in the cross section as a function of $\cos\theta^*$ at low $x_\gamma^{\rm obs}$ is stronger in the data, particularly in the photon direction. There is a sizeable contribution from a resolved photon component in both PYTHIA (35%) and HERWIG (22%). Fitting the MC distributions to the data, allowing the resolved and direct photon contributions to vary independently, results in a resolved contribution of 46% for PYTHIA and 30% for HERWIG. The fraction of charm dijet events that originates from beauty production is predicted to be $\approx 10\%$ by PYTHIA and $\approx 6\%$ by HERWIG. The shape of the beauty component is similar to that of the overall distributions.

The $x_\gamma^{\rm obs}$ distribution of CASCADE, normalised to the data, gives a larger contribution at high $x_\gamma^{\rm obs}$ and a smaller contribution at low $x_\gamma^{\rm obs}$ (Fig. 2a)). The absolute cross section predictions for CASCADE, shown in Figs. 3 – 5, are larger than the data by around 30%. This difference is concentrated in the region $x_\gamma^{\rm obs} > 0.75$ and cannot be accounted for by a variation of m_c: changing m_c to 1.3 and 1.7 GeV gave a deviation in the prediction of $\pm 10\%$. However, the CASCADE prediction reproduces the shape in $x_p^{\rm obs}$. The angular distributions are well described for $x_\gamma^{\rm obs} < 0.75$, although CASCADE underestimates the data in the proton direction (Fig. 5c). For $x_\gamma^{\rm obs} > 0.75$ (Fig. 5d), the prediction overestimates the data in all regions of $\cos\theta^*$, although the shape is described reasonably well.

7.2 Comparison with NLO QCD predictions

The differential cross sections of Figs. 2–5 have been compared to the NLO FO calculation [3]. The uncertainties in the NLO calculation, shown as the shaded area, come from the simultaneous variation of m_c between 1.3 and 1.7 GeV and μ_R between $m_T/2$ and $2m_T$. Changing the photon PDF parameterisation from AFGHO to GRVHO [32, 19], as well as varying μ_F of the photon and proton PDFs between $m_T/2$ and $2m_T$, produce small effects ($< 5\%$) on the NLO predictions.

The differential cross sections predicted by the FO calculation were corrected for hadronisation effects. For each bin, the partonic cross section was multiplied by a hadronisation correction factor, $C_{\rm had} = \sigma_{\rm MC}^{\rm hadrons}/\sigma_{\rm MC}^{\rm partons}$, which is the ratio of the MC cross sections after

and before the hadronisation process. The value of $C_{\rm had}$ was taken as the mean of the ratios obtained using HERWIG and PYTHIA. Half the spread between the two MCs was added in quadrature to the uncertainty in the NLO calculation. The deviation of $C_{\rm had}$ from unity is typically below 20% (see Tables 1-4).

Figure 2b) shows a comparison for the differential cross section in $x_\gamma^{\rm obs}$. To minimise the large migration effects at $x_\gamma^{\rm obs} > 0.75$ due to hadronisation, a wider bin than that of Fig. 2a) was used. Migrations to low $x_\gamma^{\rm obs}$ are small. The cross section can have a low $x_\gamma^{\rm obs}$ contribution at NLO due to three-parton final states in which one of the partons is treated as a photon remnant. However, the low $x_\gamma^{\rm obs}$ tail of the NLO cross section is below the data [2]. For $x_\gamma^{\rm obs} > 0.75$, the data are well described by the NLO prediction.

The differential cross section as a function of $x_p^{\rm obs}$ is compared in Fig. 3b) with the NLO FO calculation. The NLO prediction is in reasonable agreement with the data. As expected from the $x_\gamma^{\rm obs}$ comparison, the NLO prediction for the resolved-enriched $x_p^{\rm obs}$ distribution (not shown) is too low, but the shape is well reproduced.

Figures 4c-d) and 5c-d) compare the charm dijet angular distributions to the NLO calculation. For high $x_\gamma^{\rm obs}$ (Figs. 4d) and 5d)), the NLO prediction gives a good description of the data. For low $x_\gamma^{\rm obs}$ (Fig. 4c)), the NLO prediction is significantly below the data. In Fig. 5c), the NLO predicts a lower cross section than the data in both proton and photon directions. The shapes of the $|\cos\theta^*|$ and $\cos\theta^*$ distributions are reasonably well described by the NLO predictions.

8 Conclusions

The differential cross sections as a function of $\cos\theta^*$ for charm dijet photoproduction events (median $Q^2 \approx 3 \cdot 10^{-4}\,{\rm GeV}^2$) have been measured in the kinematic range $130 < W < 280\,{\rm GeV}$, $Q^2 < 1\,{\rm GeV}^2$, $p_T^{D^*} > 3\,{\rm GeV}$, $|\eta^{D^*}| < 1.5$, $E_T^{\rm jet} > 5\,{\rm GeV}$ and $|\eta^{\rm jet}| < 2.4$. The cuts on the dijet invariant mass, $M_{\rm jj} > 18\,{\rm GeV}$, and on the average jet pseudorapidity, $|\bar{\eta}| < 0.7$, select an $M_{\rm jj}$ and $|\bar{\eta}|$ region where the biases from other kinematic cuts are minimised. The distributions have been measured separately for samples of events enriched in resolved ($x_\gamma^{\rm obs} < 0.75$) and direct ($x_\gamma^{\rm obs} > 0.75$) photon processes. The angular dependence for the two samples is significantly different, reflecting the different spins of the quark and gluon propagators. The cross section rises faster with increasing $|\cos\theta^*|$ for resolved photoproduction, where processes involving spin-1 gluon exchange dominate, than for direct photoproduction, where processes involving spin-1/2 quark exchange dominate.

The shapes of the measured differential cross sections are well reproduced by PYTHIA. Except for the angular distributions at low $x_\gamma^{\rm obs}$, HERWIG gives an adequate description of

these shapes. The predictions of CASCADE describe the data at low $x_\gamma^{\rm obs}$ in both shape and normalisation. For high $x_\gamma^{\rm obs}$, the prediction significantly overestimates the data, but gives a reasonable description of the shapes. The shapes of the measured angular distributions are approximately reproduced by the NLO FO predictions. The absolute cross sections predicted by the NLO FO calculation reproduce the data for the sample enriched in direct photons but are below the data for the sample enriched in resolved photons.

Associating the D^* meson with one of the jets allows the sign of $\cos\theta^*$ to be defined. In all cases, the $\cos\theta^*$ distributions show a mild rise towards $|\cos\theta^*| = 1$, as expected from quark exchange, except for the resolved-enriched sample in which the cross section rises steeply in the photon direction ($\cos\theta^* = -1$), as expected from gluon exchange. This observation indicates that most of the resolved photon contribution in LO QCD charm production is due to charm originating from the photon, rather than to the competing resolved photon process $gg \to c\bar{c}$. This demonstrates that charm originating from the photon is the dominant component in the resolved photoproduction of dijet events with charm.

9 Acknowledgments

We thank the DESY Directorate for their strong support and encouragement. The remarkable achievements of the HERA machine group were essential for the successful completion of this work and are greatly appreciated. We are grateful for the support of the DESY computing and network services. The design, construction and installation of the ZEUS detector have been made possible owing to the ingenuity and effort of many people from DESY and home institutes who are not listed as authors. We thank H. Jung for informative discussions and S. Frixione for providing his NLO code.

References

[1] ZEUS Collaboration, M. Derrick et al., Phys. Lett. B 348 (1995) 665.

[2] ZEUS Collaboration, J. Breitweg et al., Eur. Phys. J. C 6 (1999) 67.

[3] S. Frixione et al., Nucl. Phys. B 412 (1994) 225;
S. Frixione et al., Phys. Lett. B 348 (1995) 633;
S. Frixione et al., Nucl. Phys. B 454 (1995) 3.

[4] ZEUS Collaboration, M. Derrick et al., Phys. Lett. B 384 (1995) 401;
ZEUS Collaboration, S. Chekanov et al., Eur. Phys. J. C 23 (2002) 615.

[5] OPAL Collaboration, G. Abbiendi et al., Eur. Phys. J. C 10 (1999) 547;
OPAL Collaboration, G. Abbiendi et al., Preprint hep-ex/0301013, 2003.

[6] ZEUS Collaboration, U. Holm (ed.), *The ZEUS Detector*. Status Report (unpublished), DESY (1993), available on `http://www-zeus.desy.de/bluebook/bluebook.html`.

[7] N. Harnew et al., Nucl. Inst. Meth. A 279 (1989) 290;
B. Foster et al., Nucl. Phys. Proc. Suppl. B 32 (1993) 181;
B. Foster et al., Nucl. Inst. Meth. A 338 (1994) 254.

[8] M. Derrick et al., Nucl. Inst. Meth. A 309 (1991) 77;
A. Andresen et al., Nucl. Inst. Meth. A 309 (1991) 101;
A. Caldwell et al., Nucl. Inst. Meth. A 321 (1992) 356;
A. Bernstein et al., Nucl. Inst. Meth. A 336 (1993) 23.

[9] J. Andruszków et al., Report DESY-92-066, DESY, 1992;
ZEUS Collaboration, M. Derrick et al., Z. Phys. C 63 (1994) 391;
ZEUS Luminosity Group, J. Andruszków et al., Acta Phys. Pol. B 32 (2001) 2025.

[10] W. H. Smith, K. Tokushuku and L. W. Wiggers, *Proc. Computing in High-Energy Physics (CHEP), Annecy, France, Sept. 1992*, C. Verkerk and W. Wojcik (eds.), p. 222. CERN (1992). Also in preprint DESY 92-150B.

[11] F. Jacquet and A. Blondel, *Proceedings of the Study for an ep Facility for Europe*, U. Amaldi (ed.), p. 391. Hamburg, Germany (1979). Also in preprint DESY 79/48.

[12] S. Catani et al., Nucl. Phys. B 406 (1993) 187.

[13] S.D. Ellis and D.E. Soper, Phys. Rev. D 48 (1993) 3160.

[14] Particle Data Group, D.E. Groom et al., Eur. Phys. J. C 15 (2000) 1.

[15] T. Sjöstrand et al., Comp. Phys. Comm. 135 (2001) 238.

[16] G. Marchesini et al., Comp. Phys. Comm. 67 (1992) 465;
G. Corcella et al. JHEP 0101 (2001) 010;
G. Corcella et al., Preprint hep-ph/0107071, 2001.

[17] V.N. Gribov and L.N. Lipatov, Sov. J. Nucl. Phys. 15 (1972) 438;
L.N. Lipatov, Sov. J. Nucl. Phys. 20 (1975) 94;
G. Altarelli and G. Parisi, Nucl. Phys. B 126 (1977) 298;
Yu.L. Dokshitzer, Sov. Phys. JETP 46 (1977) 641.

[18] CTEQ Collaboration, H.L. Lai et al., Eur. Phys. J. C 12 (2000) 375.

[19] M. Glück, E. Reya and A. Vogt, Phys. Rev. D 46 (1992) 1973.

[20] B.R. Webber, Nucl. Phys. B 238 (1984) 492.

[21] B. Andersson et al., Phys. Rep. 97 (1983) 31.

[22] R. Brun et al., *GEANT3, Technical Report CERN-DD/EE/84-1.* CERN, 1987.

[23] H. Jung and G. P. Salam, Eur. Phys. J. C 19 (2001) 351;
H. Jung, Comp. Phys. Comm. 143 (2002) 100;
H. Jung, J. Phys. G 28 (2002) 971.

[24] L.V. Gribov, E.M. Levin and M.G. Ryskin, Phys. Rep. 100 (1983) 1;
E.M. Levin and M.G. Ryskin, Phys. Rep. 189 (1990) 267;
E.M. Levin et al., Sov. J. Nucl. Phys. 53 (1991) 657;
E.M. Levin et al., Sov. J. Nucl. Phys. 54 (1991) 867;
S. Catani, M. Ciafaloni and F. Hautmann, Phys. Lett. B 242 (1990) 97;
S. Catani, M. Ciafaloni and F. Hautmann, Nucl. Phys. B 366 (1991) 135;
J.C. Collins and R.K. Ellis, Nucl. Phys. B 360 (1991) 3;
G. Marchesini and R.K. Webber, Nucl. Phys. B 386 (1992) 215.

[25] M. Ciafaloni, Nucl. Phys. B 296 (1988) 49;
S. Catani, F. Fiorani and G. Marchesini, Phys. Lett. B 234 (1990) 339;
S. Catani, F. Fiorani and G. Marchesini, Nucl. Phys. B 336 (1990) 18;
G. Marchesini, Nucl. Phys. B 445 (1995) 49.

[26] S.P. Baranov and N.P. Zotov, Phys. Lett. B 491 (2000) 111;
S.P. Baranov et al., Eur. Phys. J. C 24 (2002) 425.

[27] P. Aurenche, J.P. Guillet and M. Fontannaz, Z. Phys. C 64 (1994) 621.

[28] C. Peterson et al., Phys. Rev. D 27 (1983) 105.

[29] P. Nason and C. Oleari, Nucl. Phys. B 565 (2000) 245.

[30] L. Gladilin, Preprint hep-ex/9912064, 1999, (unpublished).

[31] M.G. Ryskin, A.G. Shuvaev and Yu.M. Shabelski, Phys. Atom. Nucl. 64 (2001) 120.

[32] M. Glück, E. Reya and A. Vogt, Phys. Rev. D 45 (1992) 3986.

$x_\gamma^{\rm obs}$ bin	$d\sigma/dx_\gamma^{\rm obs}$	$\Delta_{\rm stat}$	$\Delta_{\rm syst}$	$\Delta_{\rm ES}$ (nb)	$C_{\rm had}$
0.250, 0.375	0.115	± 0.029	$^{+0.037}_{-0.017}$	$^{+0.004}_{-0.001}$	0.941 ± 0.040
0.375, 0.500	0.196	± 0.055	$^{+0.064}_{-0.034}$	$^{+0.022}_{-0.005}$	0.950 ± 0.004
0.500, 0.625	0.407	± 0.082	$^{+0.101}_{-0.086}$	$^{+0.032}_{-0.029}$	1.006 ± 0.008
0.625, 0.750	1.011	± 0.102	$^{+0.073}_{-0.169}$	$^{+0.093}_{-0.112}$	1.285 ± 0.050
0.750, 0.875	2.000	± 0.147	$^{+0.159}_{-0.105}$	$^{+0.150}_{-0.159}$	
0.875, 1.000	1.727	± 0.122	$^{+0.243}_{-0.080}$	$^{+0.052}_{-0.089}$	
0.750, 1.000	1.864	± 0.096	$^{+0.145}_{-0.066}$	$^{+0.101}_{-0.124}$	0.851 ± 0.041

Table 1: *Measured cross sections as a function of $x_\gamma^{\rm obs}$. The statistical, systematic and jet energy scale ($\Delta_{\rm ES}$) uncertainties are shown separately. The multiplicative hadronisation correction applied to the NLO prediction is shown in the last column. The uncertainty shown for the hadronisation correction is half the spread between the values obtained using the HERWIG and PYTHIA models.*

$x_p^{\rm obs}$ bin	$d\sigma/dx_p^{\rm obs}$	$\Delta_{\rm stat}$	$\Delta_{\rm syst}$	$\Delta_{\rm ES}$ (nb)	$C_{\rm had}$
0.0055, 0.0110	23.28	± 2.47	$^{+2.70}_{-2.58}$	$^{+0.62}_{-0.95}$	0.799 ± 0.040
0.0110, 0.0165	36.90	± 2.96	$^{+1.95}_{-2.74}$	$^{+2.53}_{-3.05}$	0.910 ± 0.031
0.0165, 0.0220	30.72	± 2.57	$^{+2.91}_{-2.08}$	$^{+1.90}_{-2.20}$	0.953 ± 0.027
0.0220, 0.0275	18.55	± 2.05	$^{+0.97}_{-1.18}$	$^{+1.61}_{-1.49}$	0.985 ± 0.017
0.0275, 0.0330	7.84	± 1.50	$^{+0.33}_{-1.88}$	$^{+0.58}_{-0.37}$	0.984 ± 0.019
0.0330, 0.0385	3.21	± 0.77	$^{+0.56}_{-0.39}$	$^{+0.02}_{-0.41}$	1.020 ± 0.047
0.0385, 0.0440	2.37	± 0.69	$^{+0.55}_{-0.31}$	$^{+0.41}_{-0.02}$	1.022 ± 0.012

Table 2: *Measured cross sections as a function of $x_p^{\rm obs}$. For further details, see the caption to Table 1.*

$\lvert\cos\theta^*\rvert$ bin	$d\sigma/d\lvert\cos\theta^*\rvert$	$\Delta_{\rm stat}$	$\Delta_{\rm syst}$	$\Delta_{\rm ES}$ (nb)	$C_{\rm had}$
$x_\gamma^{\rm obs} < 0.75$					
0.00000, 0.10375	0.056	± 0.034	$^{+0.022}_{-0.022}$	$^{+0.014}_{-0.005}$	1.007 $\pm$ 0.014
0.10375, 0.20750	0.040	± 0.027	$^{+0.028}_{-0.010}$	$^{+0.011}_{-0.003}$	1.099 $\pm$ 0.003
0.20750, 0.31125	0.126	± 0.041	$^{+0.022}_{-0.026}$	$^{+0.011}_{-0.014}$	1.072 $\pm$ 0.026
0.31125, 0.41500	0.114	± 0.032	$^{+0.032}_{-0.025}$	$^{+0.015}_{-0.005}$	1.099 $\pm$ 0.048
0.41500, 0.51875	0.280	± 0.062	$^{+0.055}_{-0.051}$	$^{+0.027}_{-0.021}$	1.107 $\pm$ 0.041
0.51875, 0.62250	0.300	± 0.069	$^{+0.095}_{-0.059}$	$^{+0.009}_{-0.050}$	1.101 $\pm$ 0.029
0.62250, 0.72625	0.536	± 0.088	$^{+0.031}_{-0.138}$	$^{+0.005}_{-0.045}$	1.145 $\pm$ 0.014
0.72625, 0.83000	0.732	± 0.108	$^{+0.087}_{-0.155}$	$^{+0.053}_{-0.036}$	1.115 $\pm$ 0.018
$x_\gamma^{\rm obs} > 0.75$					
0.00000, 0.10375	0.277	± 0.055	$^{+0.049}_{-0.038}$	$^{+0.012}_{-0.030}$	0.923 $\pm$ 0.069
0.10375, 0.20750	0.401	± 0.065	$^{+0.037}_{-0.064}$	$^{+0.044}_{-0.030}$	0.919 $\pm$ 0.044
0.20750, 0.31125	0.471	± 0.063	$^{+0.045}_{-0.080}$	$^{+0.020}_{-0.039}$	0.910 $\pm$ 0.052
0.31125, 0.41500	0.390	± 0.070	$^{+0.055}_{-0.036}$	$^{+0.023}_{-0.028}$	0.906 $\pm$ 0.068
0.41500, 0.51875	0.584	± 0.082	$^{+0.048}_{-0.047}$	$^{+0.024}_{-0.034}$	0.876 $\pm$ 0.056
0.51875, 0.62250	0.636	± 0.089	$^{+0.044}_{-0.040}$	$^{+0.017}_{-0.030}$	0.863 $\pm$ 0.061
0.62250, 0.72625	0.810	± 0.098	$^{+0.094}_{-0.026}$	$^{+0.059}_{-0.041}$	0.832 $\pm$ 0.036
0.72625, 0.83000	0.922	± 0.126	$^{+0.105}_{-0.090}$	$^{+0.026}_{-0.046}$	0.756 $\pm$ 0.013

Table 3: *Measured cross sections as a function of* $\lvert\cos\theta^*\rvert$ *for* $x_\gamma^{\rm obs} < 0.75$ *and* $x_\gamma^{\rm obs} > 0.75$. *For further details, see the caption to Table 1.*

$\cos\theta^*$ bin	$d\sigma/d\cos\theta^*$	$\Delta_{\rm stat}$	$\Delta_{\rm syst}$	$\Delta_{\rm ES}$ (nb)	$C_{\rm had}$
$x_\gamma^{\rm obs} < 0.75$					
-0.830, -0.664	0.471	± 0.072	$^{+0.065}_{-0.077}$	$^{+0.034}_{-0.023}$	1.063 $\pm$ 0.008
-0.664, -0.498	0.198	± 0.036	$^{+0.043}_{-0.025}$	$^{+0.006}_{-0.018}$	1.065 $\pm$ 0.023
-0.498, -0.332	0.111	± 0.028	$^{+0.028}_{-0.014}$	$^{+0.012}_{-0.007}$	1.084 $\pm$ 0.029
-0.332, 0.000	0.032	± 0.011	$^{+0.009}_{-0.010}$	$^{+0.006}_{-0.003}$	1.056 $\pm$ 0.0004
0.000, 0.332	0.043	± 0.015	$^{+0.009}_{-0.007}$	$^{+0.006}_{-0.004}$	1.105 $\pm$ 0.061
0.332, 0.498	0.079	± 0.024	$^{+0.015}_{-0.021}$	$^{+0.020}_{-0.003}$	1.178 $\pm$ 0.140
0.498, 0.664	0.064	± 0.035	$^{+0.050}_{-0.028}$	$^{+0.001}_{-0.013}$	1.374 $\pm$ 0.215
0.664, 0.830	0.148	± 0.039	$^{+0.014}_{-0.038}$	$^{+0.001}_{-0.014}$	1.608 $\pm$ 0.248
$x_\gamma^{\rm obs} > 0.75$					
-0.830, -0.664	0.557	± 0.066	$^{+0.069}_{-0.054}$	$^{+0.027}_{-0.017}$	0.758 $\pm$ 0.014
-0.664, -0.498	0.371	± 0.048	$^{+0.024}_{-0.021}$	$^{+0.018}_{-0.016}$	0.842 $\pm$ 0.041
-0.498, -0.332	0.258	± 0.046	$^{+0.034}_{-0.028}$	$^{+0.017}_{-0.023}$	0.880 $\pm$ 0.053
-0.332, 0.000	0.183	± 0.024	$^{+0.022}_{-0.024}$	$^{+0.009}_{-0.017}$	0.914 $\pm$ 0.048
0.000, 0.332	0.198	± 0.024	$^{+0.018}_{-0.018}$	$^{+0.013}_{-0.017}$	0.922 $\pm$ 0.062
0.332, 0.498	0.212	± 0.035	$^{+0.029}_{-0.008}$	$^{+0.013}_{-0.008}$	0.892 $\pm$ 0.065
0.498, 0.664	0.313	± 0.053	$^{+0.024}_{-0.043}$	$^{+0.001}_{-0.023}$	0.885 $\pm$ 0.076
0.664, 0.830	0.308	± 0.068	$^{+0.031}_{-0.023}$	$^{+0.014}_{-0.019}$	0.831 $\pm$ 0.071

Table 4: *Measured cross sections as a function of* $\cos\theta^*$ *for* $x_\gamma^{\rm obs} < 0.75$ *and* $x_\gamma^{\rm obs} > 0.75$. *For further details, see the caption to Table 1.*

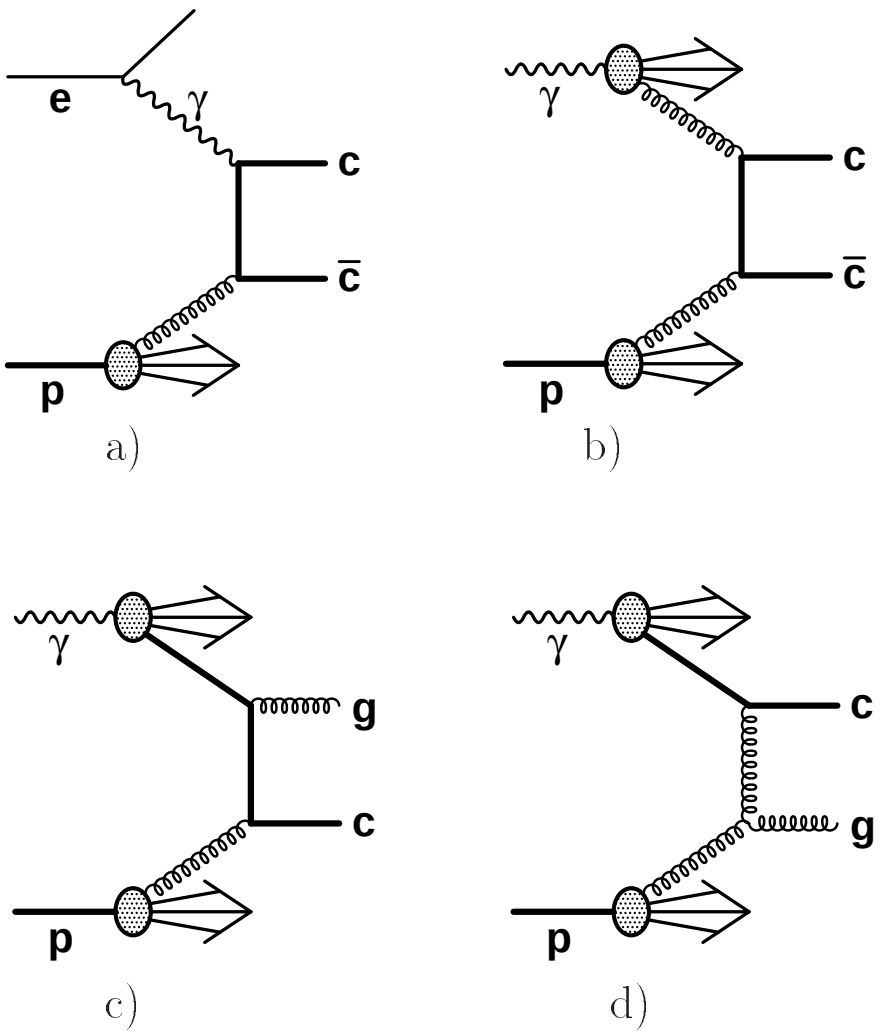

Figure 1: *LO QCD charm-production diagrams. a) direct photon: $\gamma g \to c\bar{c}$; b) resolved photon: $gg \to c\bar{c}$; c) resolved-photon charm excitation: $cg \to gc$ (c in proton hemisphere); d) resolved-photon charm excitation: $cg \to cg$ (c in photon hemisphere).*

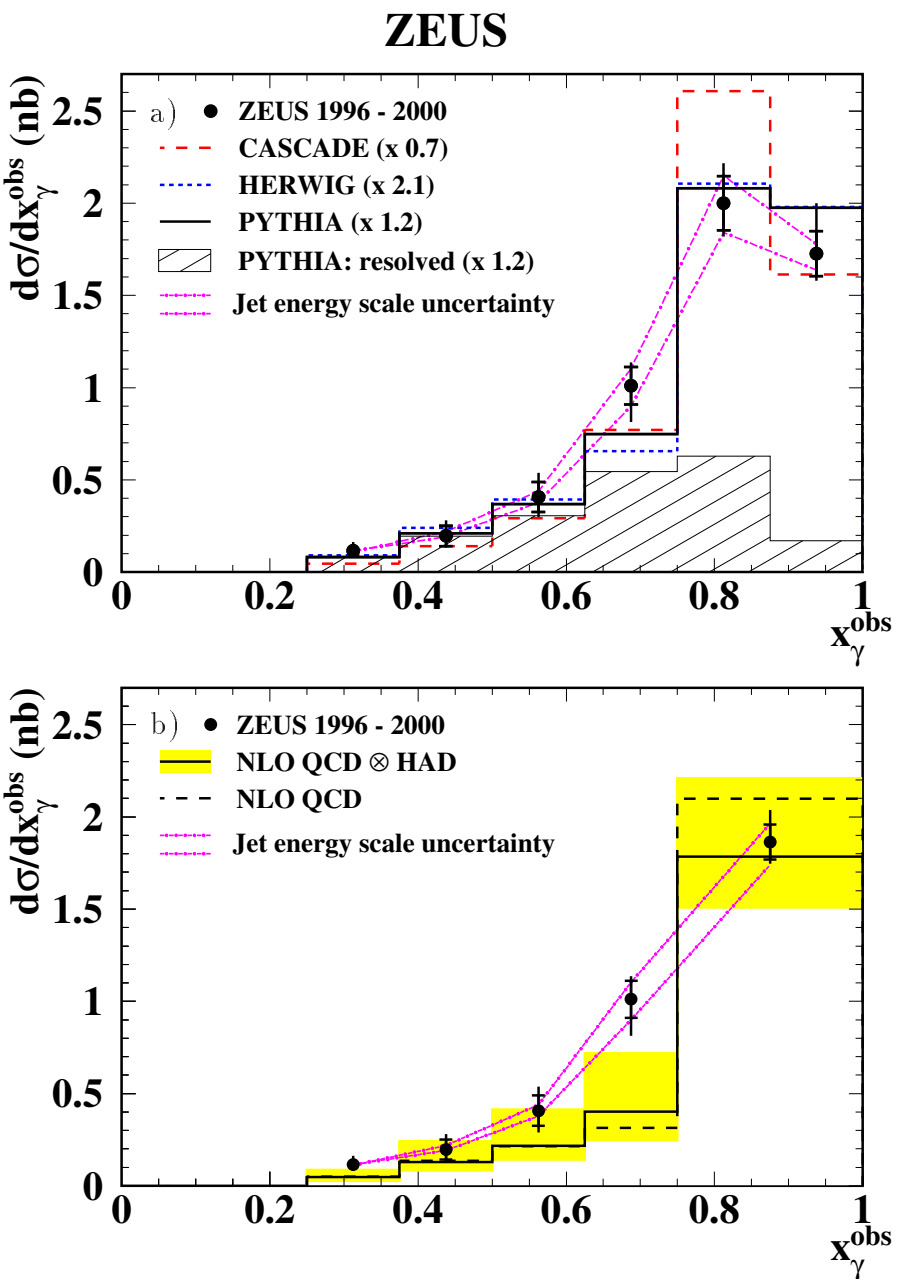

Figure 2: *Differential cross-section $d\sigma/dx_\gamma^{\rm obs}$ for the data (dots) compared with: a) various MC simulations (histograms); b) NLO FO predictions after hadronisation correction (full lines) and at parton level (dashed lines). The inner error bars show the statistical uncertainty, while the outer ones show the statistical and systematic uncertainties added in quadrature. The jet-energy-scale uncertainty is given by the two dashed-dotted lines. In a), each MC distribution is normalised to the data, as indicated in the brackets. Also shown in a) is the resolved photon distribution (hatched) of PYTHIA and in b) the uncertainty of the NLO prediction after hadronisation correction (shaded). In b) the two highest $x_\gamma^{\rm obs}$ bins have been combined.*

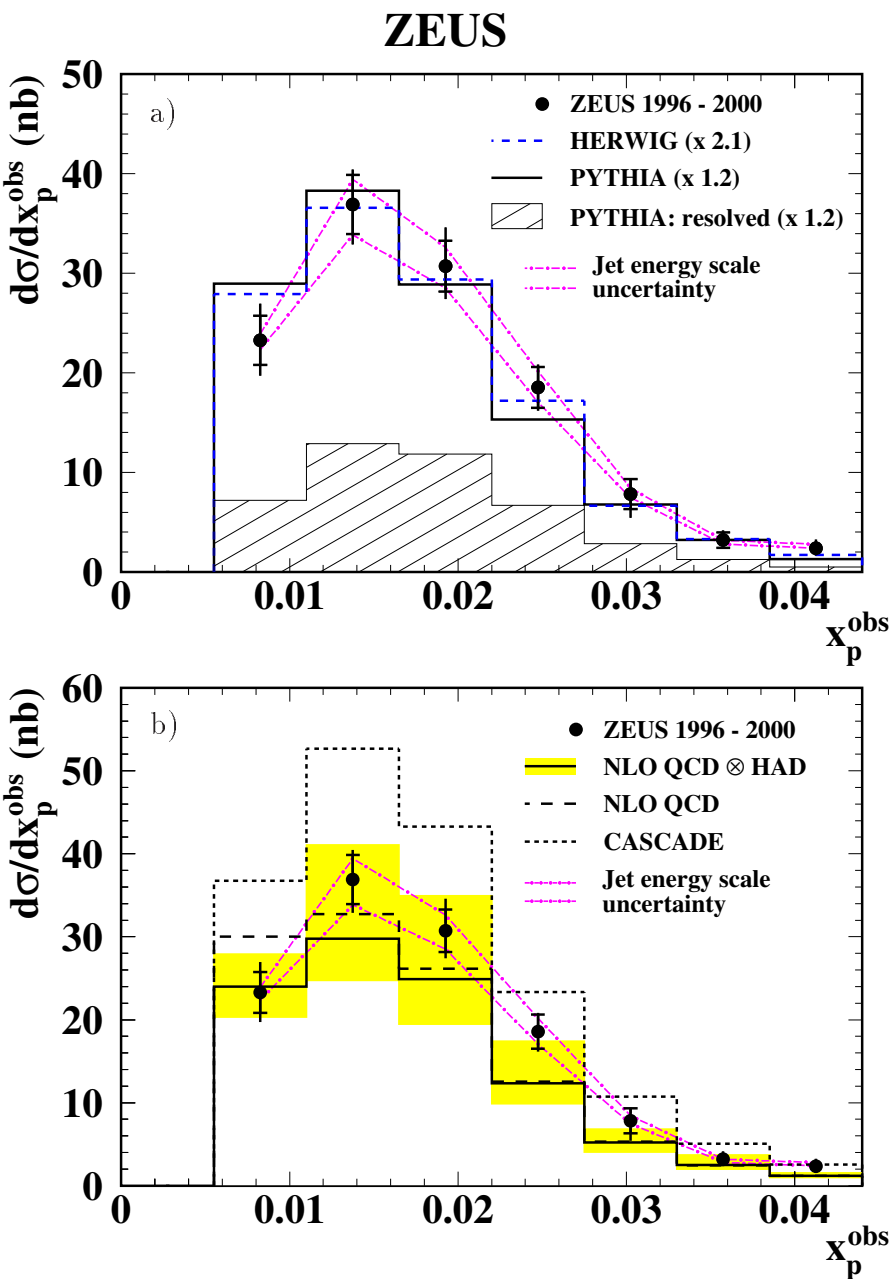

Figure 3: *Differential cross-section $d\sigma/dx_p^{\rm obs}$ for the data (dots) compared with: a) PYTHIA and HERWIG MC simulations (histograms); b) CASCADE (short-dashed lines) and NLO FO predictions after hadronisation correction (full lines) and at parton level (long-dashed lines). The inner error bars show the statistical uncertainty, while the outer ones show the statistical and systematic uncertainties added in quadrature. The jet-energy-scale uncertainty is given by the two dashed-dotted lines. In a), each MC distribution is normalised to the data, as indicated in the brackets. Also shown in a) is the resolved photon distribution (hatched) of PYTHIA and in b) the uncertainty of the NLO prediction after hadronisation correction (shaded).*

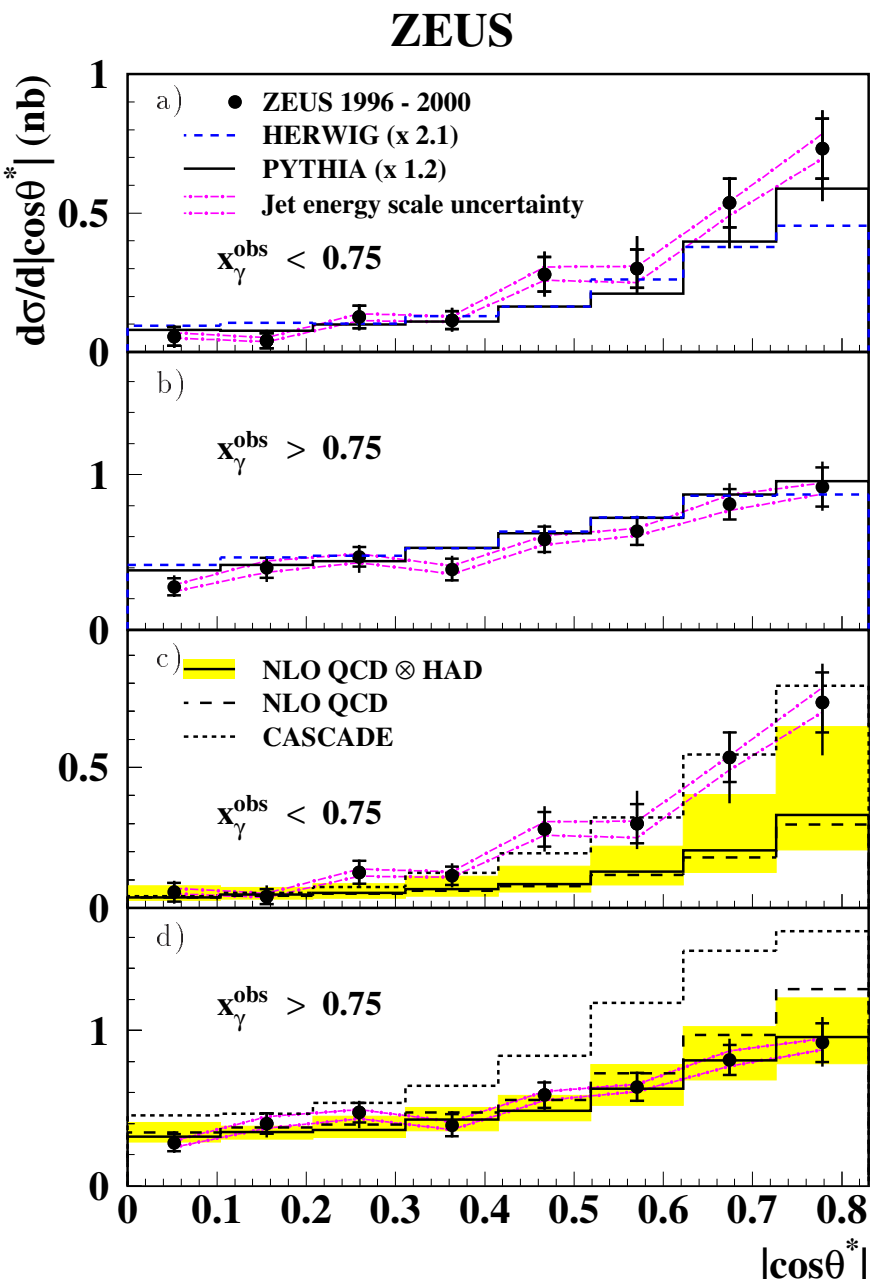

Figure 4: *Differential cross-sections $d\sigma/d|\cos\theta^*|$ (dots) compared with: a-b) PYTHIA and HERWIG MC simulations (histograms); c-d) CASCADE (short-dashed lines) and NLO FO predictions after hadronisation correction (full lines) and at parton level (long-dashed lines). Results are given separately in a,c) for samples enriched in resolved photon events and in b,d) for samples enriched in direct photon events. The inner error bars show the statistical uncertainty, while the outer ones show the statistical and systematic uncertainties added in quadrature. The jet-energy-scale uncertainty is given by the two dashed-dotted lines. In a-b), each MC distribution is normalised to the data, as indicated in the brackets. Also shown in c-d) are the uncertainties of the NLO prediction after hadronisation correction (shaded).*

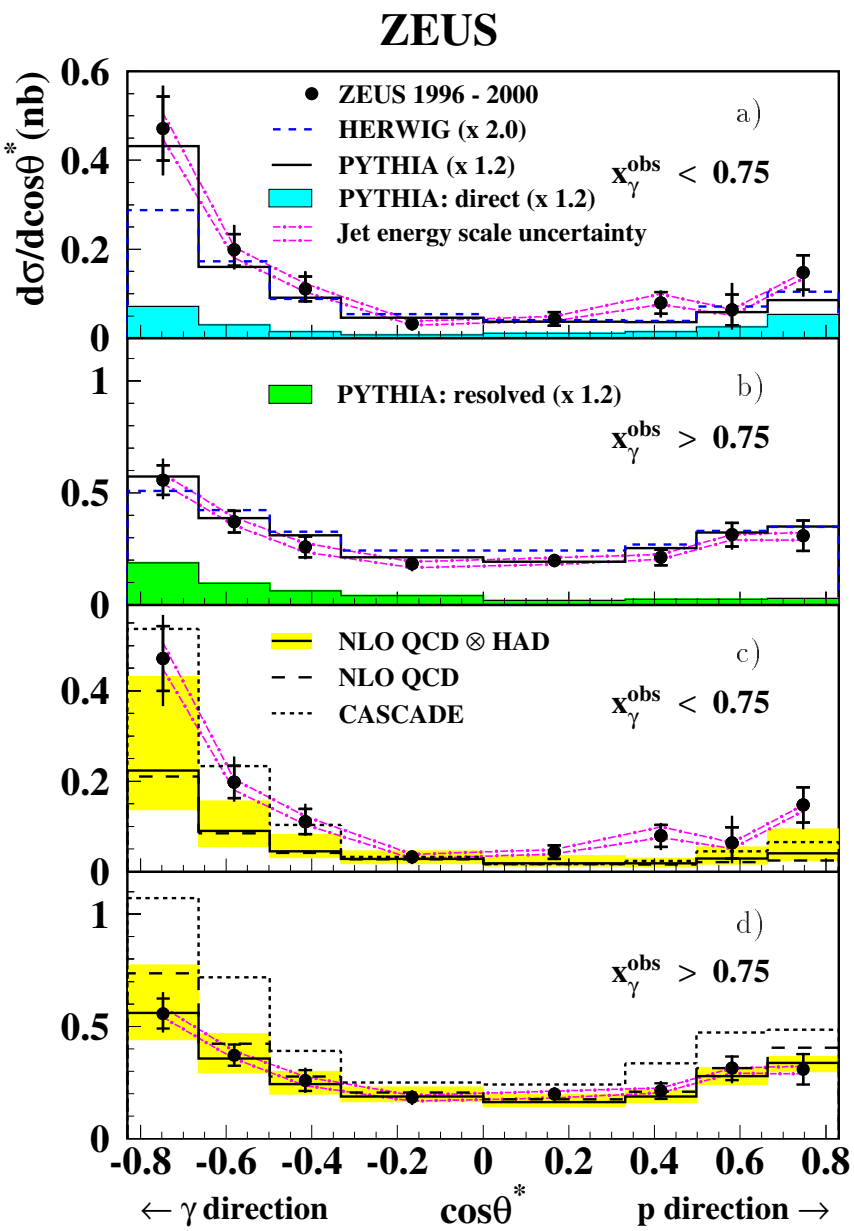

Figure 5: *Differential cross-sections $d\sigma/d\cos\theta^*$ (dots) compared with: a-b) PYTHIA and HERWIG MC simulations (histograms); c-d) CASCADE (short-dashed lines) and NLO FO predictions after hadronisation correction (full lines) and at parton level (long-dashed lines). Results are given separately in a,c) for samples enriched in resolved photon events and in b,d) for samples enriched in direct photon events. The inner error bars show the statistical uncertainty, while the outer ones show the statistical and systematic uncertainties added in quadrature. The jet-energy-scale uncertainty is given by the two dashed-dotted lines. In a-b), each MC distribution is normalised to the data, as indicated in the brackets. Also shown as shaded areas in a) and b) are the contribution of the direct photon process in PYTHIA to the resolved-enriched sample and the contribution of the resolved photon process to the direct-enriched sample, respectively. The uncertainties of the NLO prediction after the hadronisation correction are shown as the shaded areas in c) and d).*